\



Voltage-controllable magnetic skyrmion dynamics for spiking neuron device applications

Ming-Min Zhu(朱明敏), Shu-Ting Cui(崔淑婷), Xiao-Fei Xu(徐晓飞), Sheng-Bin Shi(施胜宾), Di-Qing Nian(年迪青), Jing Luo(罗京), Yang Qiu(邱阳), Han Yang(杨涪), Guo-Liang Yu(郁国良), and Hao-Miao Zhou (周浩淼)

Citation: Chin. Phys. B, 2022, 31 (**1**): 018503. DOI: 10.1088/1674-1056/ac05b0
Journal homepage: http://cpb.iphy.ac.cn; http://iopscience.iop.org/cpb

What follows is a list of articles you may be interested in

Magnetic two-dimensional van der Waals materials forspintronic devices

Yu Zhang(张雨), Hongjun Xu(许洪军), Jiafeng Feng(丰家峰), Hao Wu(吴昊), Guoqiang Yu(于国强), and Xiufeng Han(韩秀峰)

Chin. Phys. B, 2021, 30 (**11**): 118504. DOI: 10.1088/1674-1056/ac2808

Defect induced room-temperature ferromagnetism and enhanced photocatalytic activity in Ni-doped ZnO synthesized by electrodeposition

Deepika, Raju Kumar, Ritesh Kumar, Kamdeo Prasad Yadav, Pratyush Vaibhav, Seema Sharma, Rakesh Kumar Singh, and Santosh Kumar†

Chin. Phys. B, 2020, 29 (**10**): 108503. DOI: 10.1088/1674-1056/ab9c0c

Room-temperature electric control of exchange bias effect in $CoO_{1-\delta}$/Co films using $Pb(Mg_{1/3}Nb_{2/3})_{0.7}Ti_{0.3}O_3$ (110) substrates

Xin Wen(闻馨), Rui Wu(吴锐), Wen-Yun Yang(杨文云), Chang-Sheng Wang(王常生), Shun-Quan Liu(刘顺荃), Jing-Zhi Han(韩景智), Jin-Bo Yang(杨金波)

Chin. Phys. B, 2020, 29 (**9**): 098503. DOI: 10.1088/1674-1056/aba611

Homogeneous and inhomogeneous magnetic oxide semiconductors

Xiao-Li Li(李小丽), Xiao-Hong Xu(许小红)

Chin. Phys. B, 2019, 28 (**9**): 098506. DOI: 10.1088/1674-1056/ab38ac

Real-space observation of individual skyrmions in helimagnetic nanostripes

Jin Chi-Ming, Du Hai-Feng

Chin. Phys. B, 2015, 24 (**12**): 128501. DOI: 10.1088/1674-1056/24/12/128501

Voltage-controllable magnetic skyrmion dynamics for spiking neuron device applications

Ming-Min Zhu(朱明敏)[†], Shu-Ting Cui(崔淑婷)[†], Xiao-Fei Xu(徐晓飞), Sheng-Bin Shi(施胜宾), Di-Qing Nian(年迪青), Jing Luo(罗京), Yang Qiu(邱阳), Han Yang(杨洽), Guo-Liang Yu(郁国良)[‡], and Hao-Miao Zhou (周浩淼)[§]

Key Laboratory of Electromagnetic Wave Information Technology and Metrology of Zhejiang Province, College of Information Engineering, China Jiliang University, Hangzhou 310018, *China*

(Received 20 February 2021; revised manuscript received 18 May 2021; accepted manuscript online 27 May 2021)

Voltage-controlled magnetic skyrmions have attracted special attention because they satisfy the requirements for well-controlled high-efficiency and energy saving for future skyrmion-based neuron device applications. In this work, we propose a compact leaky-integrate-fire (LIF) spiking neuron device by using the voltage-driven skyrmion dynamics in a multiferroic nanodisk structure. The skyrmion dynamics is controlled by well tailoring voltage-induced piezostrains, where the skyrmion radius can be effectively modulated by applying the piezostrain pulses. Like the biological neuron, the proposed skyrmionic neuron will accumulate a membrane potential as skyrmion radius is varied by inputting the continuous piezostrain spikes, and the skyrmion radius will return to the initial state in the absence of piezostrain. Therefore, this skyrmion radius-based membrane potential will reach a definite threshold value by the strain stimuli and then reset by removing the stimuli. Such the LIF neuronal functionality and the behaviors of the proposed skyrmionic neuron device are elucidated through the micromagnetic simulation studies. Our results may benefit the utilization of skyrmionic neuron for constructing the future energy-efficient and voltage-tunable spiking neural networks.

Keywords: magnetic skyrmion, leaky-integrate-fire, multiferroic heterostructure, artificial neuron

PACS: 85.75.–d, 84.35.+i, 75.70.Kw, 75.78.Cd **DOI:** 10.1088/1674-1056/ac05b0

1. Introduction

Neuromorphic computing paradigm aiming to mimic brain-like behaviors through the implementation of artificial neural networks has achieved rapid development in the field of artificial intelligence.[1–4] Hardware implementation of such a paradigm can be used for complex pattern recognition, image processing, data classification, and other massive-parallel tasks with ultra-low energy consumption. The primary objective in emulating neurobiological behavior within an artificial system is to efficiently replicate the neuron and synapse functionalities.[5] A simple abstract model consisting of artificial neurons and synapses can be implemented in a conventional CMOS hardware, but these Si-based circuits are burdensome due to their high power consumption and area overhead. Therefore, it is crucial to find potential device structures to change the CMOS hardware by directly implementing neural and synaptic operations.[6–8]

The spintronic devices have been considered as promising candidates for future artificial neural networks by mimicking the functionality of biological neurons with nonvolatile control, which enables the effective reduction of energy consumption and heat generation during the information processing and transmission.[9–11] Among them, magnetic skyrmions have attracted special attention because of their topological nature, nanoscale size and ultra-low driving current density compared with other counterparts such as domain walls and magnetic bubbles.[12,13] Most recently, several theoretical reports have used skyrmions in artificial neurons and synapse to design neural network.[14–16] Li *et al.*[17] and Chen *et al.*[18] have used the current-driven skyrmion motion dynamics in the nanotracks to mimic the neuronal activity of a biologic neuron, in which the leaky-integrate-fire (LIF) functionality can be achieved through an electrical driving current, with the moving distance of the skyrmion indicating the membrane potential of biological neurons. Liang *et al.*[19] have also proposed an injected current modulated motion radius of skyrmion in a nanodisk to effectively implement the LIF operation. This electric current driven mechanism will bring high energy loss due to the Joule heating, and will not satisfy the requirements for well-controlled, high efficiency, and energy saving for future skyrmion-based neuron device applications.

A much more desirable option is to use voltage rather than current to drive skyrmion dynamics for artificial neuron design. Fortunately, voltage-controlled skyrmions dynamics with interfacial Dzyaloshinskii–Moriya interaction (i-DMI) has been revealed in the multiferroic heterostructures.[20,21] Although a general equation to describe the relationship between DMI constant and strain has not been established, many

[†]These authors contributed equally to this work.
[‡]Corresponding author. E-mail: glyu@cjlu.edu.cn
[§]Corresponding author. E-mail: hmzhou@cjlu.edu.cn

© 2022 Chinese Physical Society and IOP Publishing Ltd

experimental researches together with micromagnetic simulations have tried to clarify the respective roles of strain-induced changes in both perpendicular magnetic anisotropy (PMA) and i-DMI in the electric field-induced spin dynamics process.[22,23] The voltage-controlled skyrmion memristor based on a multiferroic heterostructure has also established a relationship between the magneto-resistance and skyrmion size, which shows a potential application in the neuromorphic computing.[24,25] In the present work, we propose a compact LIF spiking neuron device by using the voltage-driven skyrmion dynamics in a multiferroic nanostructure. The mechanism and behavior of skyrmion radius variation with the voltage induced piezostrain are investigated firstly. Then, this mechanism is used to realize an LIF neuronal behavior by controlling the skyrmion size variation that behaves like the membrane potential of a biological neuron. The LIF neuronal functionality and behaviors of the proposed skyrmionic neuron device are revealed through comprehensive micromagnetic simulation studies.

2. Device structure and simulation method

The skyrmionic neuron device based on a multiferroic heterostructure consisting of ferroelectric (FE) substrate/heavy metal (HM)/ferromagnetic (FM) layers is illustrated in Fig. 1. The "leaky-integrate" and "fire" neuronal behavior can be realized through the voltage control of skyrmion size on a nanodisk. Firstly, a Néel-type skyrmion is initiated in the center of the FM layer that is strongly spin-orbit coupled with the HM layer, and this coupling can provide an interfacial perpendicular magnetic anisotropy (PMA) and DMI to stabilize the skyrmion.[17,26] Then, a voltage-induced piezostrain is generated in the FE substrate and further transferred to the coupled FM layer, which makes skyrmion size vary. Therefore, to mimic the neuronal behavior, by inputting the continuous piezostrain spikes the skyrmion radius will vary like a membrane potential accumulation, and it can return to the initial state in the absence of strain input. The skyrmion size based membrane potential can reach a definite threshold value by the strain stimuli and then reset by removing the stimuli. Finally, a magnetic tunnel junction (MTJ) detection layer is used to read out the electrical signal with magnetoresistance (MR) effect, by sensing the skyrmion size variation, which makes it possible that the skyrmionic neuron can fire an output resistance spike when the skyrmion size reaches a definite threshold by continuous strain spikes.

Micromagnetic simulations are carried out by using the GPU-based software package Mumax^3, including the magnetoelastic contribution resulting from the piezostrain by applying a voltage to the FE substrate and the i-DMI contribution induced at the interface between the FM layer and the HM layer. The time-dependent magnetization dynamics is governed by the Landau–Lifshitz–Gilbert (LLG) equations containing the effective magnetic field $\boldsymbol{H}_{\rm eff}$[27]

$$\frac{\partial \boldsymbol{m}}{\partial t} = -\mu_0\gamma(\boldsymbol{m}\times\boldsymbol{H}_{\rm eff}) + \alpha\left(\boldsymbol{m}\times\frac{\partial \boldsymbol{m}}{\partial t}\right), \tag{1}$$

where $\boldsymbol{m} = \boldsymbol{M}/M_{\rm s}$ represents the spatial distribution of reduced local magnetization vector, $M_{\rm s}$ denotes the saturation magnetization α is the Gilbert damping parameter, γ is the gyromagnetic ratio, and μ_0 is the vacuum permeability. The effective field is given by $\boldsymbol{H}_{\rm eff} = -\frac{1}{\mu_0 M_{\rm s}}\frac{\partial F_{\rm tot}}{\partial \boldsymbol{m}}$, where $F_{\rm tot}$ is the total energy that contains all the interactions of the system, including the DMI energy, anisotropy energy, exchange coupling energy, demagnetizing field energy, and magneto-elastic energy. The magnetic anisotropy energy and the exchange coupling energy lead to the FM single domain state, while the DMI energy induces the helical magnetic structures.[21] Thus, the magnetic domain structure varies in the competition among these energies. The i-DMI energy contribution to $\boldsymbol{H}_{\rm eff}$ is given by[28]

$$\boldsymbol{H}_{\rm DMI} = \frac{2D}{\mu_0 M_{\rm s}}\left[(\nabla\cdot\boldsymbol{m})\,e_z - \nabla m_z\right], \tag{2}$$

where m_z is the z component of magnetization and D represents the effective i-DMI constant. For the numerical calculation of the magnetoelastic field $\boldsymbol{H}_{\rm me}$, it is convenient to use the following relation:[29]

$$\begin{aligned}\boldsymbol{H}_{\rm me} = -\frac{1}{\mu_0 M_{\rm s}}\frac{\partial}{\partial \boldsymbol{m}}\Bigg\{ & B_1\left[\left(m_x^2-\frac{1}{3}\right)\varepsilon_{xx}\right. \\ & \left.+\left(m_y^2-\frac{1}{3}\right)\varepsilon_{yy}+\left(m_z^2-\frac{1}{3}\right)\varepsilon_{zz}\right] \\ & +2B_2\left(\varepsilon_{xy}m_xm_y+\varepsilon_{yz}m_ym_z+\varepsilon_{zx}m_zm_x\right)\Bigg\},\end{aligned} \tag{3}$$

where B_1 and B_2 are the magnetoelastic coupling constants and ε_{ij} are the spatial distributions of the strain field. By numerically solving the LLG equation along with the effective field above, one can obtain the evolution of local spin distribution with time and then determine the skyrmion radius size. In our simulations, the radius of $Co_{20}Fe_{60}B_{20}$ nanodisk is fixed at $r = 250$ nm and the thickness is $t = 1$ nm. In order to investigate the strain manipulation of skyrmion size, the mesh cell dimension of 0.5 nm × 0.5 nm × 1 nm is used to discretize the model. The magnetic material parameters are adopted from previous reports[20,30] as follows: the saturation magnetization $M_{\rm s} = 1.0\times10^6$ A/m, exchange stiffness $A_{\rm ex} = 1.9\times10^{-11}$ J/m, i-DMI constant $D = 1.9$ mJ/m^2, PMA constant $K_{\rm u} = 7.85\times10^5$ J/m^3 and the damping coefficient $\alpha = 0.1$. The elastic constants $C_{11} = 2.8\times10^{11}$ N/m^2 and $C_{12} = 1.4\times10^{11}$ N/m^2, magnetostriction parameter $\lambda_{\rm s} = 3.1\times10^{-5}$, and the magnetoelastic coupling constant can be calculated from $B_1 = -3\lambda_{100}(C_{11}-C_{12})/2$.

The LIF neuronal behavior can be analogously characterized with a skyrmion-based device through the strain controlled skyrmion radius variation, and a similar membrane potential equation can be given as follows:[17]

$$Y(t) = f\left(\sum w_i(t) S_i(t) + R_0\right), \tag{4}$$

where $Y(t)$ represents the time-dependent spike event of the proposed skyrmion-based artificial neuron related to the strain-induced skyrmion radius (R_t) variation, in which skyrmion radius is defined as half of the diameter of the $m_z = 0$ contour,[31] and R_0 denotes the initial skyrmion radius. Then the LIF functionality can be realized with skyrmion radius R_t varying, and the process is described in Fig. 1. The detailed modulation of skyrmion radius and the creation of LIF behaviors in the proposed skyrmionic neuron will be expounded below.

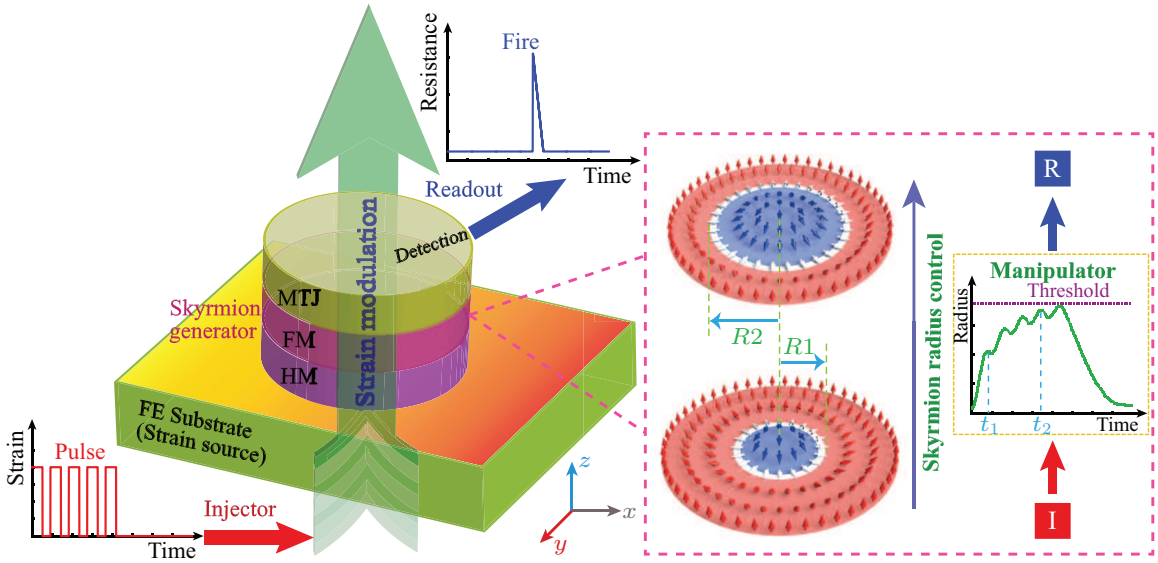


Fig. 1. Schematics of proposed spiking neuron and demonstration of LIF behaviors of skyrmion-based artificial neuron, with right panel showing Néel-type skyrmion and the time evolution of its radius.

3. Results and discussion

Figure 2 shows the effect of the out-of-plane piezostrain on the dynamic behaviors of skyrmion in the multiferroic heterostructure. The initial skyrmion with a radius of 41.5 nm is generated in the center of the nanodisk by minimizing the total energy. With different time-varying strain fields exerted on the nanostructure, the variations of skyrmion radius are calculated and shown in Fig. 2(a). With a critical time T_c, the skyrmion radius can be enlarged to a maximum value of R_{max} by the sustained strain contribution, and after this critical time the skyrmion radius will keep constant. The detailed strain dependent maximum radius R_{max} and critical time T_c is shown in Fig. 2(b). It is found that the R_{max} is proportional to the applied strain. However, there is a local maximum value of the threshold time T_c when the negative strain increases to about -2000 ppm as shown in Fig. 2(b). When the negative strain $|\varepsilon| < 2000$ ppm, the critical time T_c increases as the strain value rises, showing an opposite trend for the strain $|\varepsilon| > 2000$ ppm. In fact, the skyrmion is confined in the nanodisk, and its radius variation is a result of the competition between the driving force and the repulsive force from the boundary. When the driving strain is small, the boundary force may take the major role to prevent the skyrmion from enlarging, leading the critical time to extend. By increasing the driving strain enough to exceed the boundary repulsive force, the total effective driving force will increase and the critical time will shorten.

The time-dependent strain pulse is given in Fig. 3(a), and the time dependence of total energy and the skyrmion radius are presented in Figs. 3(b) and 3(c). During the exerting a -2000 ppm strain on the nanodisk, the skyrmion radius increases to a maximum value in a critical time, with the applied strain driven, as discussed above. By removing the strain, the skyrmion radius will gradually return to the initial state as a result of the boundary repulsive force effect. In this dynamic process, the total energy of the system will decrease with the skyrmion approaching to the initial state. Therefore, the skyrmion radius will return back to the initial value without applying the strain. Such an expanding and shrinking dynamic behavior of skyrmion radius driven by the strain can be used to perform the neuronal LIF spiking operation. Considering the skyrmion radius as the membrane potential, the skyrmion radius becomes larger with the inputting of the spike strain, exhibiting a "integrate" behavior; besides, the skyrmion will return to its original state by removing the strain, showing a "leaky" behavior. These "integrate" and "leaky" behaviors can be further controlled to realize the artificial neuron activity by continuously injecting the spike strain as discussed below.

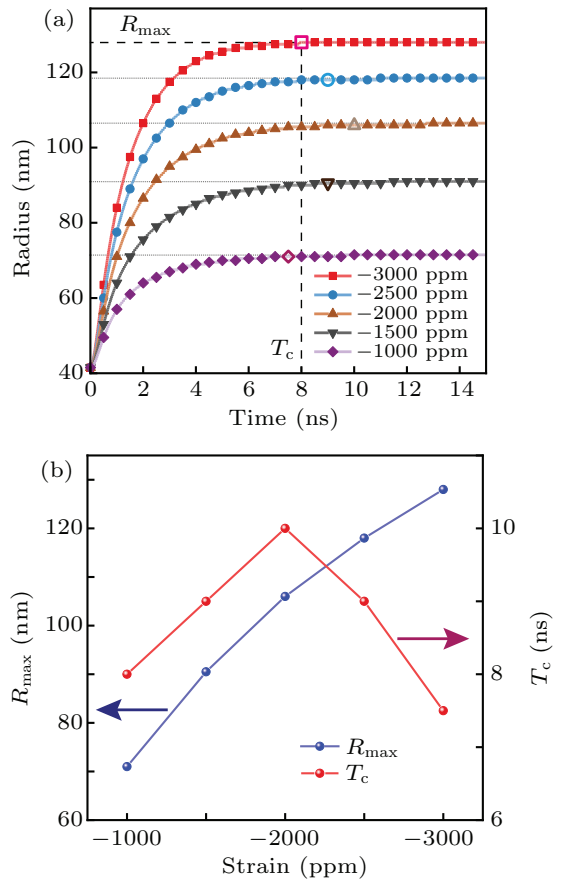


Fig. 2. (a) Micromagnetic simulation of the skyrmion radius variations with time for different strains exerted on nanodisk and (b) maximal radius of skyrmion R_{max} and critical time T_c *versus* applied out-of-plane strain.

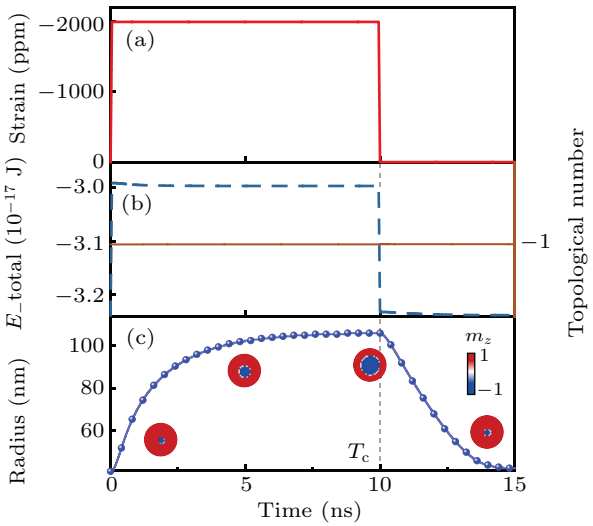


Fig. 3. Strain, total energy, topological number, and skyrmion radius varying with time, with inset showing snapshots of the simulations, where the component of magnetization is color coded.

To further verify the feasibility of the design of skyrmionic neuron device based on the multiferroic heterostructure, different spike strains are used to simulate the response of the skyrmion. Figure 4 shows the micromagnetic simulation results of the skyrmion-based artificial neuron under two kinds of input strain signals, *i.e.*, periodic homogeneous square wave and inhomogeneous square wave. It is obvious that the LIF operation can be realized in the proposed skyrmionic neuron device with all types of input strain signals. With the changing of the amplitude of each strain pulse, the intensity of "integration" will increase for a pulse with stronger amplitude, which makes the threshold value for the artificial neuron easily defined. On the other hand, we can also control the amount of "integration" by modulating the action time of each strain pulse (not shown here) and realize a quick fire response in the skyrmion based neuron device.

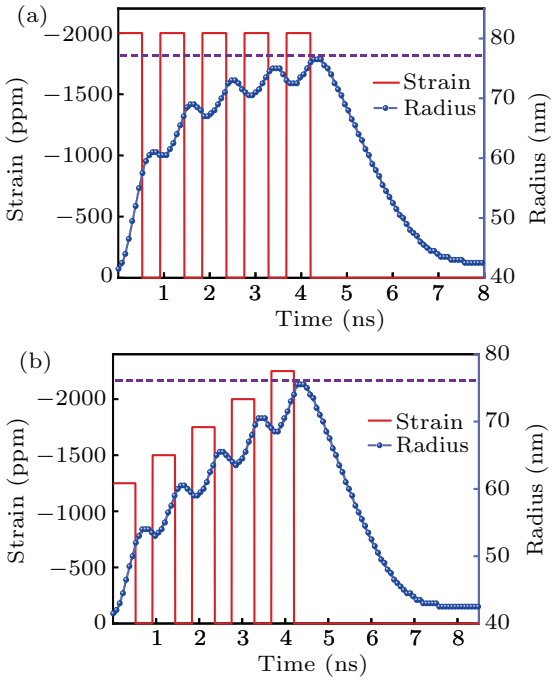


Fig. 4. Skyrmion radius varying with time under the strain pulses for (a) homogeneous square wave and (b) inhomogeneous square wave with frequency of 1.09 GHz.

In practice, two important factors should be taken into consideration in designing the artificial neuron device: one is the stochastic input spikes and the other is the fast reset operation. The LIF processes with respect to the time for both skyrmion radius variations under homogeneous and inhomogeneous input strain spikes are exhibited in Fig. 4. To investigate the totally stochastic input spike strain effect on the skyrmion radius, a train of strain pulses with random amplitudes and frequencies is used to drive the dynamic variation of skyrmion radius, and an obvious LIF behavior can also be observed in Fig. 5(a). It is worth noting that a reset strain with a reverse direction to that of the input spike strain is explored to pursue a fast reset operation, as shown in Fig. 5(b). Just with 1000-ppm positive strain pulse acting on the reset process, the reset time can be shortened from 3.79 ns to 1.74 ns, more than half time being reduced in comparison with the natural reset process shown in Fig. 5(a). In addition, this single device implementation of artificial neuron can be realized in a reverse skyrmion dynamics by controlling positive strain spikes to dwindle the radius, which may enhance the possibilities for utilizing the skyrmionic neuron device.

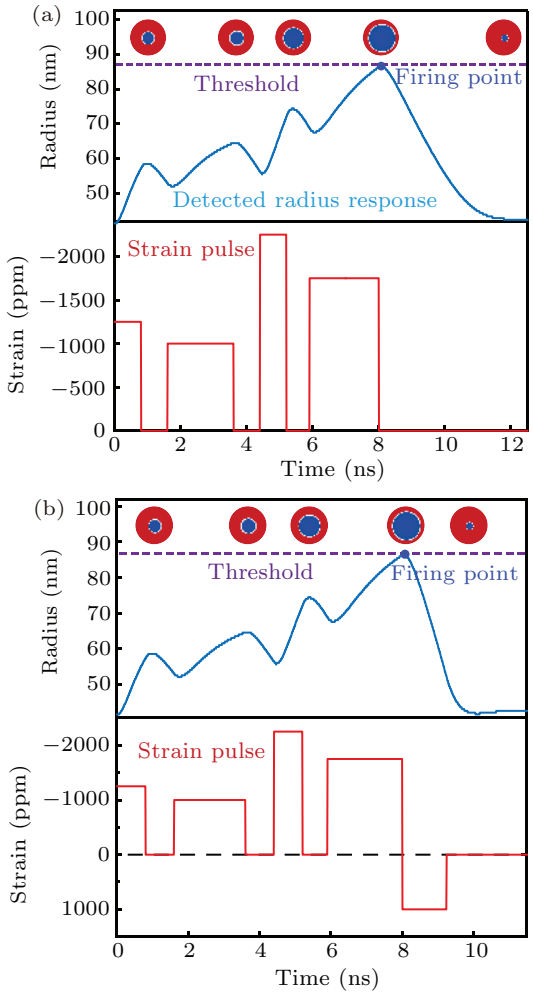


Fig. 5. Creation of LIF functionality of the skyrmionic neuron device under different strategies: (a) skyrmion radius enlargement driven by stochastic input strain signal with natural reset process, and (b) skyrmion radius enlargement driven by the stochastic input strain signal through applying a positive strain pulse during the reset process.

4. Conclusions

In this work, a compact LIF spiking neuron device by using the voltage-driven skyrmion dynamics in a multiferroic nanodisk structure is proposed. The voltage-induced piezostrains are used to modulate the skyrmion radius variation, and an expanding and shrinking dynamic behavior of skyrmion radius can be realized with different types of input strain signals. The detailed LIF neuronal functionality and behaviors of the proposed skyrmionic neuron device are well expounded through the comprehensive micromagnetic simulation studies. Our results provide a new route for realizing voltage-controllable skyrmionic neuron in future energy-efficient and tunable neuromorphic computing hardware.

Acknowledgements

Project supported by the National Natural Science Foundation of China (Grant Nos. 11902316, 51902300, and 11972333) and the Natural Science Foundation of Zhejiang Province, China (Grant Nos. LQ19F010005, LY21F010011, and LZ19A020001).

References

[1] Zhang D, Zeng L, Cao K, Wang M, Peng S, Zhang Y, Zhang Y, Klein J O, Wang Y and Zhao W 2016 *IEEE Trans. Biomed. Circuits Syst.* **10** 828
[2] Hirohata A, Yamada K, Nakatani Y, Prejbeanu I L, Diény B, Pirro P and Hillebrands B 2020 *J. Magn. Magn. Mater.* **509** 166711
[3] Yang K, Malhotra A, Lu S and Sengupta A 2020 *IEEE Trans. Electron Dev.* **67** 1340
[4] Wang C, Wang Z, Wang M, Zhang X, Zhang Y and Zhao W 2020 *IEEE Trans. Electron Dev.* **67** 2621
[5] Brigner W H, Friedman J S, Hassan N, Jiang-Wei L, Hu X, Saha D, Bennett C H, Marinella M J, Incorvia J A C and Garcia-Sanchez F 2019 *IEEE Trans. Electron Dev.* **66** 4970
[6] Merolla P A, Arthur J V, Alvarez-Icaza R, Cassidy A S, Sawada J, Akopyan F, Jackson B L, Imam N, Guo C, Nakamura Y, Brezzo B, Vo I, Esser S K, Appuswamy R, Taba B, Amir A, Flickner M D, Risk W P, Manohar R and Modha D S 2014 *Science* **345** 668
[7] Akopyan F, Sawada J, Cassidy A, Alvarez-Icaza R, Arthur J, Merolla P, Imam N, Nakamura Y, Datta P, Nam G, Taba B, Beakes M, Brezzo B, Kuang J B, Manohar R, Risk W P, Jackson B and Modha D S 2015 *IEEE Trans. Computer-Aided Design Integr. Circuits Syst.* **34** 1537
[8] Lee D, Kwak M, Moon K, Choi W, Park J, Yoo J, Song J, Lim S, Sung C and Banerjee W 2019 *Adv. Electron. Mater.* **5** 1800866
[9] Grollier J, Querlioz D, Camsari K Y, Everschor-Sitte K, Fukami S and Stiles M D 2020 *Nat. Electron.* **3** 360
[10] Fukami S and Ohno H 2018 *J. Appl. Phys.* **124** 151904
[11] Sengupta A, Shim Y and Roy K 2017 *IEEE Trans. Biomed. Circuits Syst.* **10** 1152
[12] Fert A, Reyren N and Cros V 2017 *Nat. Rev. Mater.* **2** 17031
[13] Zhang X, Zhou Y, Mee Song K, Park T E, Xia J, Ezawa M, Liu X, Zhao W, Zhao G and Woo S 2020 *J. Phys.: Condens. Matter* **32** 143001
[14] Chen M C, Sengupta A and Roy K 2018 *IEEE Trans. Magn.* **54** 1500207
[15] Azam M A, Bhattacharya D, Querlioz D and Atulasimha J 2018 *J. Appl. Phys.* **124** 152122
[16] Prychynenko D, Sitte M, Litzius K, Krüger B, Bourianoff G, Kläui M, Sinova J and Everschor-Sitte K 2018 *Phys. Rev. Appl.* **9** 014034
[17] Li S, Kang W, Huang Y, Zhang X, Zhou Y and Zhao W 2017 *Nanotechnology* **28** 31LT01
[18] Chen X, Kang W, Zhu D, Zhang X, Lei N, Zhang Y, Zhou Y and Zhao W 2018 *Nanoscale* **10** 6139
[19] Liang X, Zhang X, Xia J, Ezawa M, Zhao Y, Zhao G and Zhou Y 2020 *Appl. Phys. Lett.* **116** 122402
[20] Yanes R, Garcia-Sanchez F, Luis R F, Martinez E, Raposo V, Torres L and Lopez-Diaz L 2019 *Appl. Phys. Lett.* **115** 132401
[21] Li Z, Zhang Y, Huang Y, Wang C, Zhang X, Liu Y, Zhou Y, Kang W, Koli S C and Lei N 2018 *J. Magn. Magn. Mater.* **455** 19
[22] Wang Y, Wang L, Xia J, Lai Z, Tian G, Zhang X, Hou Z, Gao X, Mi W, Feng C, Zeng M, Zhou G, Yu G, Wu G, Zhou Y, Wang W, Zhang X X and Liu J 2020 *Nat. Commun.* **11** 3577
[23] Ba Y, Zhuang S, Zhang Y, Wang Y, Gao Y, Zhou H, Chen M, Sun W, Liu Q, Chai G, Ma J, Zhang Y, Tian H, Du H, Jiang W, Nan C, Hu J M and Zhao Y 2021 *Nat. Commun.* **12** 322
[24] Luo S, Xu N, Guo Z, Zhang Y, Hong J and You L 2019 *IEEE Electron Dev. Lett.* **40** 635
[25] Yu Z, Shen M, Zeng Z, Liang S, Liu Y, Chen M, Zhang Z, Lu Z, You L, Yang X, Zhang Y and Xiong R 2020 *Nanoscale Adv.* **2** 1309
[26] Tang J, Kong L, Wang W, Du H and Tian M 2019 *Chin. Phys. B* **28** 087503
[27] Zhang S L, Wang W W, Burn D M, Peng H, Berger H, Bauer A, Pfleiderer C, van der Laan G and Hesjedal T 2018 *Nat. Commun.* **9** 2115
[28] Dong D, Cai L, Li C, Liu B, Li C and Liu J 2019 *J. Phys. D: Appl. Phys.* **52** 295001
[29] Wang Q, Domann J, Yu G, Barra A, Wang K L and Carman G P 2018 *Phys. Rev. Appl.* **10** 034052
[30] Voto M, Lopez-Diaz L and Martinez E 2017 *Sci. Rep.* **7** 13559
[31] Hu J M, Yang T and Chen L Q 2020 *Acta Mater.* **183** 145